Structural basis for the inhibition of poxvirus assembly by the antibiotic rifampicin

Damià Garriga[a,b,1,2], Stephen Headey[c,1], Cathy Accurso[a,b], Menachem Gunzburg[c], Martin Scanlon[c], and Fasséli Coulibaly[a,b,3]

[a]Infection and Immunity Program, Biomedicine Discovery Institute, Monash University, Melbourne, VIC 3800, Australia; [b]Department of Biochemistry and Molecular Biology, Monash University, Melbourne, VIC 3800, Australia; and [c]Monash Institute of Pharmaceutical Sciences, Monash University, Melbourne, VIC 3052, Australia

Edited by Bernard Moss, National Institute of Allergy and Infectious Diseases, National Institutes of Health, Bethesda, MD, and approved July 12, 2018 (received for review June 19, 2018)

Poxviruses are large DNA viruses that cause disease in animals and humans. They differ from classical enveloped viruses, because their membrane is acquired from cytoplasmic membrane precursors assembled onto a viral protein scaffold formed by the D13 protein rather than budding through cellular compartments. It was found three decades ago that the antibiotic rifampicin blocks this process and prevents scaffold formation. To elucidate the mechanism of action of rifampicin, we have determined the crystal structures of six D13–rifamycin complexes. These structures reveal that rifamycin compounds bind to a phenylalanine-rich region, or F-ring, at the membrane-proximal opening of the central channel of the D13 trimer. We show by NMR, surface plasmon resonance (SPR), and site-directed mutagenesis that A17, a membrane-associated viral protein, mediates the recruitment of the D13 scaffold by also binding to the F-ring. This interaction is the target of rifampicin, which prevents A17 binding, explaining the inhibition of viral morphogenesis. The F-ring of D13 is both conserved in sequence in mammalian poxviruses and essential for interaction with A17, defining a target for the development of assembly inhibitors. The model of the A17–D13 interaction describes a two-component system for remodeling nascent membranes that may be conserved in other large and giant DNA viruses.

poxvirus | rifampicin | X-ray crystallography | membrane remodeling | virus assembly

Viruses of the Nucleo Cytoplasmic Large DNA Viruses (NCLDV) group, proposed as a new order *Megavirales* (1), have a complex morphogenesis that involves the formation of a characteristic internal membrane. Unlike enveloped viruses that bud through cellular membranes, these viruses assemble their lipid bilayer in the cytoplasm of infected cells onto an external protein scaffold (2–4). In most NCLDVs, this scaffold represents the capsid shell of the infectious particles. Poxviruses are atypical among NCLDVs, because they lose the protein scaffold, undergo large-scale structural rearrangements, and adopt a distinctive brick-shaped morphology that departs from the organization of other virions (2, 5). Despite these differences, D13, the protein that forms the scaffold, is homologous to the double-barrel capsid proteins that enclose the membrane in the infectious capsids of other NCLDVs (6, 7). In keeping with this homology, D13 has the ability to self-assemble into a honeycomb lattice and if tethered to lipids in vitro, to remodel membranes into spherical particles in the absence of other viral proteins (6). In vivo, D13 functions together with a set of viral proteins coined Viral Membrane Assembly Proteins to generate and assemble membrane precursors derived from the endoplasmic reticulum into viral crescents and ultimately, immature virions (8). These membrane precursors are open-ended tubular structures (9, 10) that adopt a pronounced curvature resulting, at least in part, from the reticulon-like action of the viral protein A17 (11). A17 is also necessary to recruit D13 to the viral membranes (12, 13).

In the prototype poxvirus, vaccinia virus (VACV), morphogenesis can be arrested by rifampicin before membrane assembly (14, 15). The inhibition is independent of the antibiotic activity of rifampicin, which targets the bacterial DNA-dependent RNA polymerases (16). The effect is reversible, and assembly resumes within minutes on withdrawal of rifampicin (14, 15). Rifampicin has not been used as an antiviral drug in a clinical context because of its low potency and the rapid emergence of rifampicin-resistant mutant viruses (17, 18). However, the antibiotic has been an invaluable tool to understand VACV assembly. Study of viruses that grow despite the presence of rifampicin has identified mutations in the *D13L* gene, which was hence called the rifampicin resistance gene (19–21). The phenotype of recombinant viruses where the expression of *D13L* is repressed is very similar to the effect of rifampicin (22), suggesting that rifampicin functions by inactivating the function of the D13 protein. In both cases, virus-induced membranes form, but they adopt aberrant tubular structures instead of the crescent-shaped precursors of immature virions (22). An alternative resistance mechanism to rifampicin has been described more recently where the gene of A17 is duplicated, further supporting a critical role for the interaction between D13 and A17 in the formation of the viral membrane (23).

Here, we investigate the molecular interactions leading to the recruitment of D13 to viral membrane precursors and the inhibition of this process by rifampicin. Using X-ray crystallography, surface plasmon resonance (SPR), NMR spectroscopy, and site-directed mutagenesis, we show that D13 is indeed the target of rifampicin in poxvirus and characterize the binding of rifampicin and its derivatives. We also show that D13 binds to the first 16 residues of the membrane-associated A17 protein. Site-directed mutagenesis

Significance

Most antibiotics do not interfere with viral infections. Rifampicin is a notable exception, as it inhibits several poxviruses, including the causative agent of smallpox. However, the inhibition of viral assembly is unrelated to the antibacterial activity of rifampicin against microbial RNA polymerases. Here, we reveal how the antibiotic prevents the recruitment of an essential scaffolding protein to nascent viral membranes. Based on these results, we provide a structural model of membrane assembly that is distinct from budding through cellular membranes and is most likely conserved in many large DNA viruses. Together, the mechanism of membrane assembly and structural models provide avenues to develop broad spectrum inhibitors against human and animal poxviruses.

Author contributions: M.S. and F.C. designed research; D.G., S.H., C.A., and M.G. performed research; D.G., S.H., M.S., and F.C. analyzed data; and D.G., S.H., M.S., and F.C. wrote the paper.

The authors declare no conflict of interest.

This article is a PNAS Direct Submission.

Data deposition: The atomic coordinates and structure factors have been deposited in the Protein Data Bank, www.wwpdb.org (PDB ID codes 6BEB–6BEI).

[1]D.G. and S.H. contributed equally to this work.

[2]Present address: XAIRA Beamline, ALBA Synchrotron Light Source, 08290 Barcelona, Spain.

[3]To whom correspondence should be addressed. Email: Fasseli.Coulibaly@monash.edu.

This article contains supporting information online at www.pnas.org/lookup/suppl/doi:10.1073/pnas.1810398115/-/DCSupplemental.

Published online August 1, 2018.

reveals that the binding site of A17 on D13 overlaps with the rifampicin binding site. Competition assays confirm that rifampicin targets this interaction, displacing A17 from D13, thereby inhibiting the tethering of D13 to the nascent viral envelope and explaining its mechanism of action by steric occlusion of the F-ring.

Results and Discussion

Rifampicin Blocks the Membrane-Proximal Channel of the D13 Trimer. D13 was identified as a target of rifampicin over three decades ago (24), but the mode of action of this inhibitor has remained unclear. Three different mechanisms have been proposed for the rifampicin inhibition of the assembly of viral membranes: (*i*) a destabilization of the D13 protein, resulting in its aggregation in inclusion bodies (25); (*ii*) an inhibition of D13 self-assembly into a honeycomb scaffold (20); and (*iii*) prevention of the tethering of D13 to viral membranes (12, 13).

We tested whether rifampicin binds D13 using biophysical methods. Initial evidence of binding was provided by ligand-detected NMR, which provides a robust means to observe protein–ligand interactions over a wide range of affinities. Saturation transfer difference (STD) NMR experiments can be used to identify ligands that bind to a protein by observing differences in the intensity of ligand resonances in ^{1}H-NMR spectra that are acquired either with or without selective excitation of the protein (26). "On-resonance" saturation of D13 ^{1}H NMR resonances at −1.5 ppm resulted in a decrease in the intensity of rifampicin resonances compared with a spectrum acquired with "off-resonance" saturation applied at 33 ppm, indicating that rifampicin binds to D13 (*SI Appendix*, Fig. S1*A*). Binding was confirmed by recording 1D ^{1}H NMR spectra of rifampicin in the absence and presence of D13 using a Carr–Purcell–Meiboom–Gill (CPMG) sequence as a T2 relaxation filter. Small molecules tumble rapidly in solution and have long T2 relaxation times, which give rise to sharp lines in their NMR spectra. Conversely, larger proteins, such as D13, have short T2 relaxation times, which result in line broadening for resonances in their spectra. If a ligand binds a protein with an affinity in the micromolar range, such that it is in fast intermediate exchange on the NMR timescale, the effective relaxation rate is the weighted average of the population states and their relaxation times, causing a generalized broadening of the ligand resonances (27). Therefore, T2 filtered experiments, such as CPMG, can be used to identify fragments that bind to a protein via changes in their T2 relaxation. The addition of D13 at a concentration of 5–200 μM rifampicin caused a dramatic reduction in the intensity of the ^{1}H NMR resonances of rifampicin in CPMG spectra, confirming that rifampicin binds to D13 (*SI Appendix*, Fig. S1*B*).

To determine the affinity of the interaction, we immobilized the D13 trimer on an SPR sensor chip via its N-terminal hexahistidine purification tags and injected rifampicin in a concentration series. The resulting sensorgrams show rapid association–dissociation kinetics that were fit to an equilibrium binding model with an equilibrium dissociation constant $K_d = 19 \pm 5$ μM (mean ± SD) (Table 1 and *SI Appendix*, Fig. S1 *C* and *D*). The micromolar affinity of the rifampicin–D13 interaction is in good agreement with the pharmacological window of 90–240 μM reported in infected cells (18, 28).

To understand the binding of rifampicin at a molecular level, the structure of the D13–rifampicin complex was determined by X-ray crystallography to a resolution of 2.70 Å (Fig. 1 and *SI Appendix*, Table S1). Binding of rifampicin does not disrupt the overall structure of D13 or the organization of the trimer; apo and rifampicin-bound D13 trimers have an all-atom rmsd of 0.259 Å. This absence of significant changes in the D13 trimer surfaces that are involved in the honeycomb scaffold implies that rifampicin does not affect the ability of D13 to self-assemble, which suggests that the rifampicin inhibition of viral membrane assembly is not due to either of the first two hypothetical modes of action described above. Indeed, rifampicin has no detectable effect on honeycomb lattice formation in in vitro assembly (6).

As anticipated, the binding mode of rifampicin to D13 is unrelated to the interaction with bacterial RNA polymerases (29). The D13 trimer binds a single molecule of rifampicin within a central channel that runs along the threefold symmetry axis of the trimer (Fig. 1 and *SI Appendix*, Fig. S2). The antibiotic binds at the membrane-proximal end of the D13 channel, around which most of the mutations that confer resistance to rifampicin have been mapped (7, 21). Rifampicin forms a plug at the entrance of the central channel, with the planar surface of the naphthoquinone core occupying most of the channel and the C3 branch facing outward. The naphthoquinone core is slightly too large to fit face on into the channel and adopts a tilt of 26° from the plane orthogonal to the threefold axis. The interaction with D13 relies on a high surface complementarity, which buries 545 Å^2 of the solvent-exposed area of rifampicin, representing 60% of its molecular surface.

Interestingly, the chain connecting both sides of the naphthoquinone core, termed the "ansa bridge," faces the inner side of the channel. It mediates the only polar interaction between rifampicin and D13 but only indirectly through a water bridge with residue Glu165$_A$. The limited contacts made by the ansa chain differ from its critical role in docking to the bacterial RNA polymerase (29).

On the D13 side, most of the interactions are mediated by hydrophobic contacts with a phenylalanine-rich ring (F-ring) composed of residues Val24, Phe168, Pro483, Phe486, and Phe487. The ansa chain interacts with residues Val24$_B$, Phe168$_A$, Phe168$_C$, Pro483$_A$, Phe486$_A$, Phe486$_B$, Phe486$_C$, and Phe487$_A$ of the F-ring, while the napthoquinone core and the piperazine branch interact with residues Phe486$_B$ and Phe486$_A$, respectively (Fig. 1 *B* and *D* and *SI Appendix*, Table S2).

To verify the binding mode, we independently mutated each of the F-ring residues Phe168, Phe486, and Phe487 to alanine and assessed the ability of the resulting F-ring mutants to bind rifampicin by SPR. The D13 mutants were immobilized in series on SPR sensor chips with wild-type D13 to compare their binding affinities for rifampicin. All three D13 mutants showed >10-fold reduction in binding affinity compared with wild-type D13 (Fig. 1*E*, Table 1, and *SI Appendix*, Fig. S3). The reduced affinity of rifampicin binding is likely due to the absence of the phenylalanine side chains themselves rather than a global disruption of the D13 structure, since all mutants produced soluble trimers that are indistinguishable from wild-type D13 by size exclusion chromatography and negative stain electron microscopy. The crystal structure of the F$_{486}$A mutant (*SI Appendix*, Fig. S3 and

Table 1. Equilibrium dissociation constant of D13 with rifampicin or A17 peptides (mean ± SD)

K_d, μM	D13	D13$_{F168A}$	D13$_{F486A}$	D13$_{F487A}$
Rifampicin	19 ± 5 (n = 13)	205 ± 41 (n = 7)	285 ± 21 (n = 6)	198 ± 30 (n = 5)
A17$_{1–16}$	55 ± 17 (n = 7)	558 ± 138 (n = 5)	395 ± 49 (n = 5)	567 ± 74 (n = 4)
A17$_{1–8}$	119 ± 10 (n = 6)	258 ± 70 (n = 5)	324 ± 61 (n = 4)	278 ± 65 (n = 3)
A17$_{9–16}$	>1,000	>1,000	>1,000	>1,000

Values are the mean of n independent measurements ± SD.

MICROBIOLOGY

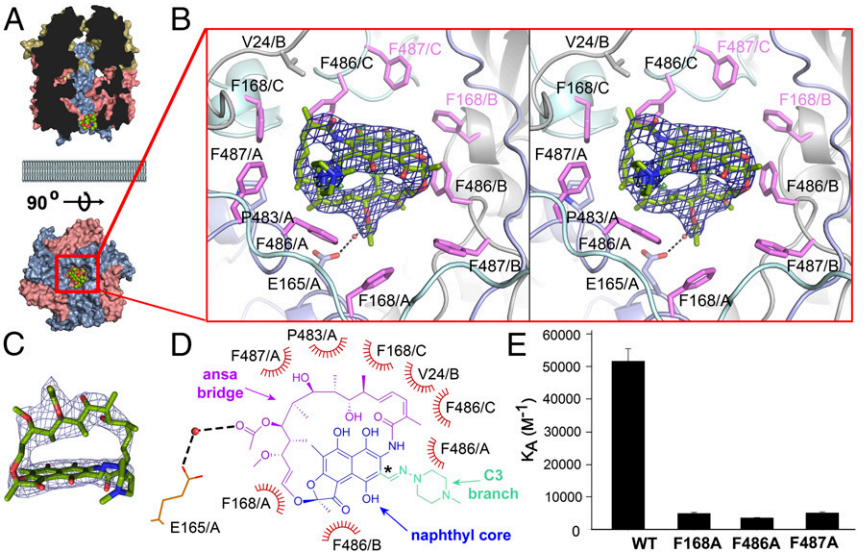

Fig. 1. Rifampicin occludes the membrane-proximal entrance of the D13 central channel. (*A*) Orthogonal views of a D13 trimer with the rifampicin molecule shown as spheres. The N- and C-terminal jelly rolls and head domain are colored in blue, red, and yellow, respectively. The crescent membrane is shown in gray. (*B*) Stereoview of the rifampicin binding site. Side chains of residues in contact with rifampicin are shown as sticks. Phenylalanine residues of the F-ring are colored pink. In rifampicin, C, O, and N atoms are colored in green, red, and blue, respectively. The 2Fo-Fc and Fo-Fc electron density maps are shown as blue and green/red meshes contoured at 1σ and +3σ/−3σ. (*C*) Side view of rifampicin. (*D*) The rifampicin binding site modified from LigPlot+. The naphtoquinone core is colored in dark blue; ansa bridge is in purple, and C3 piperazine branch is in turquoise. An asterisk indicates the C3 carbon. (*E*) SPR equilibrium binding constants of rifampicin for D13 wild-type and F-ring mutants. Error bars are SEMs.

Table S1) confirmed the absence of significant structural rearrangement beyond the loss of the phenylalanine side chain.

C3-Rifamycin Derivatives also Bind to the F-Ring of D13. Rifampicin belongs to a family of antibiotics called rifamycins. Other available rifamycins modified at the C3 position did not have improved potency against VACV compared with rifampicin (*SI Appendix*, Table S2) and were not pursued further as antivirals. Hence, we tested their ability to bind D13 using the previously described biophysical methods. The binding of the rifamycins to D13 was initially detected using CPMG NMR (*SI Appendix*, Fig. S4). Crystal structures of D13 in complex with the rifamycin derivatives confirmed that all compounds bind at the same location in the trimer (Fig. 2). SPR was used to determine the affinities of the rifamycins, which range from 19 to 246 μM, with rifampicin and rifaximin displaying the highest-affinity interactions (*SI Appendix*, Fig. S5 and Table S2). The derivatives only differ chemically from each other by the length and flexibility of the substitution at position C3 of the core. With the exception of rifabutin, these differences only induce minor changes in the contacts between each drug and D13 (Fig. 2*C*). The binding mode of rifabutin differs from the other derivatives, with a tilt angle of the naphthoquinone core with respect to the plane orthogonal to the symmetry axis of the D13 trimer channel of 60° instead of 16°–27°. This tilt is apparently forced by the bulkier and more rigid C3 branch of rifabutin that does not fit within the D13 trimer in the other mode of binding. As a result of the tilt, the C3 branch of rifabutin projects outward from the channel in the direction of the membrane. However, interactions with the F-ring on the inner side of the D13 channel are conserved in all complexes (Fig. 2). Overall, binding to the F-ring emerges as an important feature of rifamycin derivatives that is not affected by modification at the C3 and C4 positions. The lack of additional contacts through the C3 substitutions correlates with the absence of improvement in the potency of these compounds but provides options to modulate the solubility and toxicity of rifamycin derivatives. By contrast, the ansa bridge penetrates deeply into the channel, which is lined with highly conserved residues (Fig. 2*D* and *SI Appendix*, Fig. S6). Thus, modification of the ansa bridge provides unexplored opportunities to engineer molecules with increased potency. These molecules have not been developed as antibiotics because of the absolute requirement of the ansa bridge in rifamycin–RNA polymerase interactions (29).

The N-Terminal Tail of A17 Recruits D13 to Nascent Membranes by Direct Interaction. Rifampicin binds to a conserved region of D13 that is not directly involved in the honeycomb lattice formation.

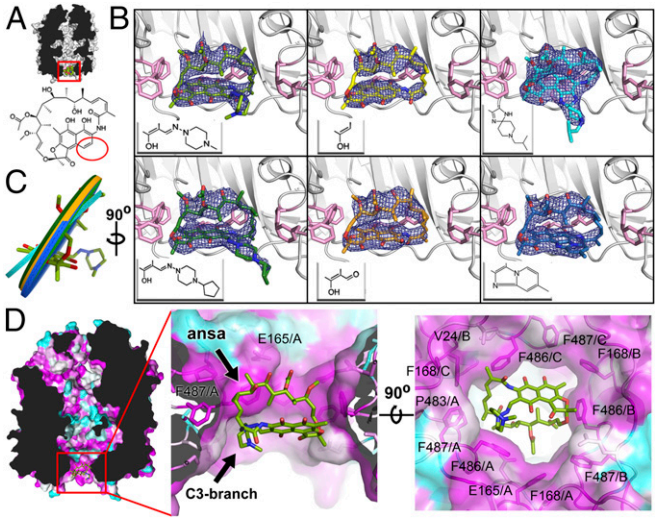

Fig. 2. The C3–rifamycin derivatives bind to the F-ring of D13. (*A*, *Upper*) Central slab through the D13 trimer. (*A*, *Lower*) Diagram of the rifamycin core with positions C3 and C4 circled in red. (*B*) Rifamycin derivatives with carbon atoms shown in light green (rifampicin), yellow (rifamycin SV), cyan (rifabutin), dark green (rifapentine), orange (3-formyl rifamycin), and dark blue (rifaximin). The 2Fo-Fc electron density map (1σ) is shown as a blue mesh. (*Insets*) Diagrams of the C3 branches. (*C*) A disk centered at the molecule centroid and aligned with the plane of the ansa bridge represents each derivative. (*D*) Surface representation of D13 colored by sequence conservation in chordopoxviruses with a pink–white–cyan gradient from high to low conservation.

This result supports the hypothesis that the antibiotic prevents an interaction between D13 and a viral or cellular partner. The viral protein A17 is the only protein known to interact with D13. The 203-residue protein is composed of a central hydrophobic segment buried in the membrane and flanked with short cytoplasmic N- and C-terminal tails corresponding to residues 1–60 and 160–203, respectively. A17 is processed by the viral protease I7 at AGX sequence motifs at positions 16 and 186 during the transition from immature to mature virions. In infected cells, D13 coimmunoprecipitates with A17 in an interaction that involves the first 38 residues of A17 (12, 13), but it is not known whether this interaction requires additional viral or cellular proteins.

We used CPMG NMR to show that a peptide corresponding to residues 1–38 of A17 ($A17_{1–38}$) binds to D13 in the absence of other viral or cellular proteins. For this, a series of ^{1}H NMR data was acquired from solutions containing 40 μM peptide both in the presence and in the absence of 10 μM D13. Binding to D13 enhances the rate of T2 relaxation for the peptide, which is manifest as a reduction in signal intensity observed in the CPMG spectrum in the presence of D13 (*SI Appendix*, Fig. S7). The minimal sequence required for binding to D13 was further refined as $A17_{1–8}$ or N-terminal acetylated $A17_{2–8}$ ($aceA17_{2–8}$), which along with $A17_{1–38}$ and $A17_{1–16}$, gives a positive response in the CPMG experiments. To establish that the changes in intensity observed in the CPMG experiments were due to relaxation-induced line broadening after protein binding rather than differences in experimental conditions (e.g., peptide concentration differences between samples, poor shimming for one of the samples), we performed a ratio-of-ratios calculation. In these experiments, two spectra with different CPMG relaxation periods (10 and 210 ms) were recorded on samples of one of the A17 peptides ($aceA17_{2–8}$; 200 μM) in the absence and presence of D13 (10 μM). From these data, we determined a relaxation factor ($f = I_{210}/I_{10}$, where I_x is the intensity of a peak in the CPMG spectrum recorded with a relaxation period of x ms) for the sample in the presence and absence of D13. The ƒ ratio is used to distinguish relaxation induced by binding from experimental variables that could potentially cause a change in the signal intensity, with a reduction >0.2 in the f ratio in the presence of protein considered as evidence of binding (27). This analysis revealed that, in the absence of D13, $aceA17_{2–8}$ has a relaxation factor $f_{apo} = 0.77$, whereas in the presence of D13, the relaxation factor decreases to $f_{protein} = 0.46$, providing clear evidence of binding. Conversely, peptides corresponding to the region downstream of residue 8 show little to no binding to D13 (Fig. 3 *A* and *B*). SPR analysis confirms these binding patterns with detectable binding for $A17_{1–38}$, $A17_{1–16}$, $A17_{1–8}$, and $aceA17_{2–8}$ but not $A17_{9–16}$. The $A17_{1–16}$ and $A17_{1–8}$ peptides have equilibrium dissociation constants for D13 in the midmicromolar range ($K_d = 55 \pm 17$ and 119 ± 10 μM, respectively) (Fig. 3*C*, Table 1, and *SI Appendix*, Fig. S8).

The $A17_{1–38}$ peptide contains three tyrosine residues in its N-terminal region at positions 3, 6, and 7, with aromatic resonances that can be identified from their H^{δ}-H^{ε} cross-peaks in 2D NOESY spectra. All three tyrosine residues are strongly affected by binding to D13, with a large attenuation of their H^{ε} and H^{δ} resonances evident in the CPMG spectrum of $A17_{1–38}$ (*SI Appendix*, Fig. S7). This concurs with their essential role first identified in infected cells by Unger et al. (13). To further evaluate the role of specific residues in the N-terminal tail of A17, we performed SPR and CPMG NMR binding experiments using a set of $A17_{1–8}$ peptides with alanine mutations at positions that are highly conserved across poxviruses (*SI Appendix*, Fig. S9). The simultaneous mutation of Tyr_6 and Tyr_7 (Y_6A/Y_7A) leads to a complete loss of peptide binding (Fig. 3 and *SI Appendix*, Fig. S10). Point mutation of either residue of the dityrosine motif also results in a more than fivefold reduction in relative binding affinity for the Y_6A and Y_7A mutants relative to wild-type $A17_{1–8}$ as determined by SPR (Fig. 3*D*), which is consistent with a reduction in the attenuation of their Tyr H^{ε} and H^{δ} resonances in CPMG NMR spectra. Binding affinities are reduced

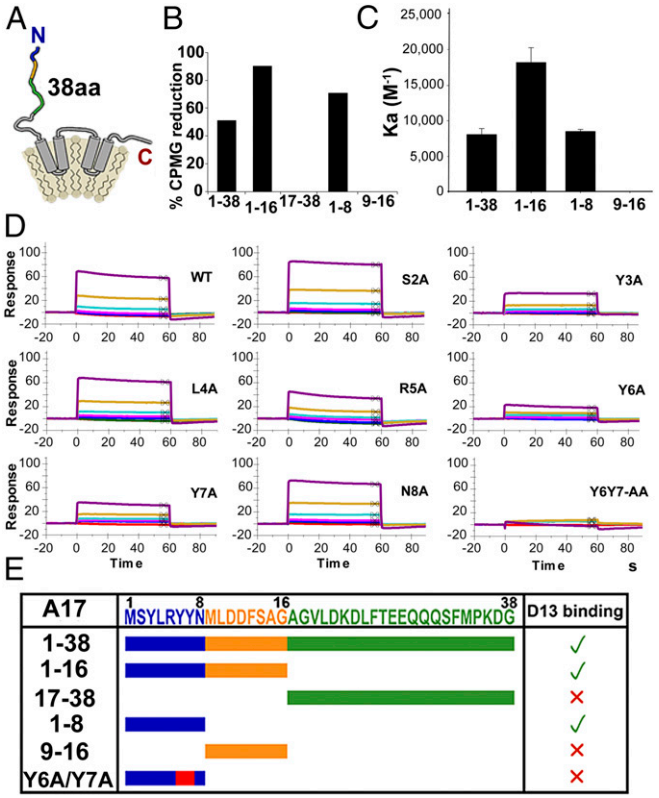

Fig. 3. The N-terminal tail of A17 binds D13. (*A*) Schematic of A17 with the viral membrane precursor shown in brown. Peptides in blue and orange are located before the I7 protease cleavage site. The rest of the $A17_{1–38}$ peptide is colored in green. (*B*) Relative reduction in CPMG signal, indicating binding to D13. (*C*) SPR equilibrium binding of D13 with peptides derived from the N terminus of A17. (*D*) SPR sensorgrams showing interaction of $A17_{1–8}$ point mutants with D13 immobilized on a sensor chip. Injections were performed in threefold serial dilutions from 200 μM. (*E*) Summary of CPMG NMR and SPR experiments assessing the determinants of the A17–D13 interaction.

five- and fourfold for the Y_3A and R_5A mutants, respectively. By contrast, mutations of other conserved residues at positions M_1A, S_2A, L_4A, and N_8A have binding to D13 similar to the wild type (*SI Appendix*, Fig. S10*C*). To test whether the initiator methionine is removed during the normal infectious cycle, SPR was performed on $A17_{2–8}$ peptides with and without acetylation. The $aceA17_{2–8}$ had a similar affinity to $A17_{1–8}$, suggesting that both an unprocessed A17 and an acetylated, truncated A17 may be compatible with productive assembly (*SI Appendix*, Fig. S10*D*).

The in vitro interaction between D13 and A17 characterized here resolves previous conflicting results obtained in a cellular context. Two previous studies (12, 13) found that residues 1–16 are required for the formation of crescents and immature virions but dispensable for coimmunoprecipitation of D13 in the absence of active viral replication. Our results indicate that the N-terminal tail of A17 is necessary and sufficient to mediate an interaction between A17 and D13. This finding concurs with rescue experiments (12, 13) and supports the hypothesis that nonnative motifs are present in N-terminally truncated A17 in the absence of normal membrane precursors of viral crescents (13). The binding affinity of A17 for D13 is relatively weak, but the interaction is likely to be strengthened by avidity effects. In vivo, each hexameric D13 ring in the honeycomb lattice is effectively tethered to viral membranes by up to six individual A17-mediated interactions. For the entire immature virion, this represents up to ~4,500 A17–D13 tethers.

MICROBIOLOGY

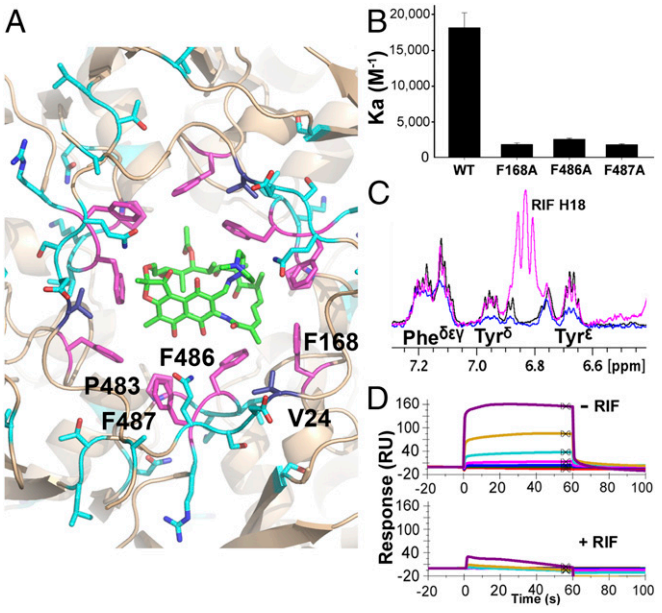

Fig. 4. A17 and rifampicin have overlapping binding sites in D13. (*A*) Residues mutated in at least one rifampicin-resistant virus in Charity et al. (21) are shown in cyan. The F-ring is shown in pink, except for V24 (blue), which is the only F-ring residue mutated in a rifampicin resistance virus. (*B*) SPR equilibrium binding constants for $A17_{1–16}$ with F-ring mutants of D13. (*C*) CPMG spectra with the aromatic region of the ^{1}H NMR spectra for $A17_{1–38}$ at 40 μM (black), $A17_{1–38}$ in the presence of 10 μM D13 (blue), and $A17_{1–38}$ in the presence of 10 μM D13 and 500 μM rifampicin (pink). The H18 resonance of rifampicin and peaks corresponding to Phe$^{\delta}$/Phe$^{\varepsilon}$/Phe$^{\zeta}$, Tyr$^{\delta}$, and Tyr$^{\varepsilon}$ hydrogens in A17 are labeled. The $A17_{1–38}$ signals are attenuated by D13 in the absence of rifampicin but not in the presence of rifampicin, which is consistent with the peptide being displaced from D13 by rifampicin. (*D*) SPR sensorgrams showing the $A17_{1–38}$ binding to D13 with (*Lower*) and without 200 μM rifampicin (*Upper*).

A17 Binds to the F-Ring of D13. The rifampicin binding site is highly conserved in sequence across chordopoxviruses, including all poxviruses infecting vertebrates (Fig. 2*D* and *SI Appendix*, Fig. S6), which suggests a possible functional role in viral morphogenesis. Mapping of spontaneous and induced mutants selected to resist the effect of rifampicin (21) reveals that the F-ring is invariant, despite the selective pressure. While most of these rifampicin-escape mutations are located in or around the central channel of D13, only 1 of 32 mutations is within the F-ring (the mutation $V_{24}F$). None affect the three phenylalanine residues of the F-ring, despite their prominent role in rifampicin binding (Fig. 4*A*). Instead, mutations cluster on either side of the Phe_{486}-Phe_{487} sequence, with nine different escape mutations in immediate proximity of this motif at positions 480, 484, 485, and 488.

Thus, we hypothesized that the F-ring region of D13 may also participate in the A17–D13 interaction. Crystals of the A17–D13 complex reveal electron density in proximity of the F-ring within the central channel. This additional electron density is not present in the D13 or D13–rifampicin structures, but the quality of the map does not allow modeling of the peptide. Notwithstanding, we were able to show the effects of the disruption of the F-ring by point mutations of D13 residues on A17 binding assessed by SPR and NMR. Compared with wild-type D13, the $F_{168}A$, $F_{486}A$, and $F_{487}A$ D13 mutants have binding affinities for $A17_{1–16}$ that are 7- to 10-fold weaker as determined by SPR (Fig. 4*B*, Table 1, and *SI Appendix*, Fig. S11). This is consistent with a reduction in the attenuation of the Tyr H$^{\varepsilon}$ and H$^{\delta}$ resonances of $A17_{1–38}$ in CPMG NMR spectra recorded in the presence of $F_{168}A$ and $F_{486}A$ relative to wild-type D13. Taken together, the structural and biophysical data show that both rifamycins and A17 rely on the F-ring to bind D13.

Rifampicin Inhibits the Interaction Between D13 and A17. To determine the impact of rifampicin on the A17–D13 interaction, competition assays were performed using NMR and SPR. Addition of rifampicin to the $A17_{1–38}$–D13 complex results in an increase in the intensity of the A17 resonances in the CPMG spectrum (Fig. 4*C*), which is consistent with dissociation of the A17 peptide from D13. Similar results were obtained for other rifamycins (*SI Appendix*, Fig. S12). The inhibition of A17 binding by rifampicin was confirmed by SPR experiments. The measured SPR response is proportional to the mass of ligand interacting with the surface-bound target. Hence, if A17 and rifampicin showed independent binding, we should expect to see additive SPR responses on coinjection. Conversely, if rifamycin inhibits A17 peptide binding to D13, a reduction in SPR response is predicted. This was indeed observed; the coinjection of 200 μM rifampicin with 0–200 μM $A17_{1–8}$, $A17_{1–16}$, or $A17_{1–38}$ caused a reduction in the observed SPR response, showing that rifampicin inhibits the binding of the A17 N-terminal tail to D13 (Fig. 4*D* and *SI Appendix*, Fig. S8).

Model of the Role of A17 and D13 in the Assembly of Crescents and Immature Virions. A structural model of early steps in poxvirus membrane assembly can be constructed that integrates structural and biophysical data obtained on both A17 and rifampicin. The $A17_{1–38}$ peptide lacks significant secondary structure as evidenced by a ^{1}H-^{1}H NOESY NMR spectrum, which has a notable absence of interresidue NOEs, including H^N-H^N cross-peaks (*SI Appendix*, Fig. S13), along with an independent study using circular dichroism showing that the region 18–50 of A17 adopts a random coil (30). With A17 in an extended conformation, the D13 channel accommodates 6 residues of the A17 peptide before reaching its narrowest constriction formed by residue Lys_{169} or ∼15 residues if the peptide inserts into the entire channel. At the constriction, the side chains of Lys_{169} are 12 Å apart, which is likely to prevent further translocation of A17 into the channel. This arrangement places residues Y_6Y_7 of A17 in proximity with the F-ring of D13 (Fig. 5), which would explain the critical role of the dityrosine motif observed in vitro (Fig. 3) and in infected cells (13). Alternatively, binding to D13 could stabilize or induce a hairpin conformation of the N terminus of A17, which would present the Y_6Y_7 motif to D13 without complete insertion. In both configurations, the recognition sites for the I7 protease formed by residues $A_{15}G_{16}$ and $A_{17}G_{18}$ are located 7 residues away from the exit of the channel and separated by 42 residues

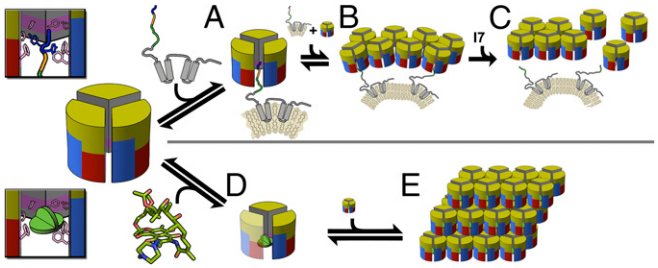

Fig. 5. Model of the D13–A17 complex formation and its inhibition by rifampicin. Schematic representation of a D13 trimer colored as in Fig. 1. (*A*–*C*) During poxvirus infection, D13 binds to the N-terminal tyrosine residues of A17 through its F-ring (*A*, *Upper Left Inset*). This interaction tethers the D13 trimers to the membrane, where they assemble into a honeycomb scaffold that drives membrane assembly into crescents and immature virions (*B*). On cleavage of A17 by the viral I7 protease, the D13 scaffold is released from the immature virion, allowing further maturation to produce infectious particles (*C*). (*D* and *E*) In the presence of rifampicin, the antibiotic plugs the F-ring (*D*, *Lower Left Inset*), blocking the interaction of D13 with A17. This prevents incorporation of D13 onto the viral membrane, leading to the accumulation of D13 trimers in inclusion bodies (*E*).

from the lipid membrane. This spacing is compatible with the steric requirements of the I7 protease to catalyze the cleavage of A17 at this site, leading to the release of the D13 layer after the immature virion is formed, a prerequisite for subsequent maturation steps (12, 13, 30).

Based on this model, the mechanism of action of rifampicin involves inhibition of the D13 recruitment at the site of viral membrane formation by steric occlusion of the membrane-proximal channel. Although an allosteric model of inhibition cannot be formally excluded, the absence of conformational differences away from the F-ring in the structures of apo D13, the D13–rifamycin complexes, and $D13_{F486A}$ makes such a mechanism unlikely.

Because the ability of D13 to self-assemble is not affected by rifampicin, unregulated self-assembly results in the formation of inclusion bodies of D13 observed in infected cells (25, 31) and the concomitant failure of membranes to assemble into crescents and immature particles in the absence of the D13 scaffold (Fig. 5). Given the low affinity of rifampicin for its target, the equilibrium is easily shifted toward an A17-bound state if rifampicin is removed or if A17 expression is increased, as seen in mutant viruses where the A17 gene has been duplicated (23). This shift allows the recruitment of D13 at A17-enriched membranes, and assembly resumes within minutes. Due to avidity effects, the transition between soluble D13 and the honeycomb lattice is likely to be cooperative on reinitiation of assembly.

This model of immature virion morphogenesis relies on a two-component system where both A17 and D13 are required for remodeling of nascent membranes. Homologs of D13 have been identified in most viruses of the proposed order *Megavirales*, but homologs of the smaller A17 protein are yet to be identified. It will be interesting to see if the model presented here extends to other large and giant DNA viruses.

Conclusions

The N-terminal tail of the A17 peptide tethers nascent viral membranes to the D13 scaffold protein during immature virion formation by binding to the D13 F-ring located at the opening of the central channel of the trimer. The antiviral activity of rifampicin arises from it binding to the F-ring, thereby blocking the interaction of D13 with A17 and preventing immature virion formation. The high conservation of the F-ring across mammalian poxviruses and its apparent inability to mutate in response to rifampicin inhibition make it an attractive target for the development of broad spectrum inhibitors against poxviruses causing disease in animals and humans.

Experimental Procedures

Detailed methods are available in *SI Appendix*. Crystals of complex were obtained by soaking or cocrystallization in 3.5–4.0 M sodium formate and 0.1 M citric acid, pH 4.8. Structures were solved by molecular replacement using Protein Data Bank ID code 3SAM (6). NMR data were collected on a Bruker AVANCE 600-MHz magnet fitted with a CryoProbe. STD spectra were acquired with 3 s of saturation at −1.5 ppm (on resonance) and 33.3 ppm (off resonance) with 200 μM rifampicin and 5 μM D13. CPMG spectra with 40–100 ms mixing time were acquired with or without 5 μM D13. For A17 binding and competition assays, CPMG spectra were acquired with a relaxation delay of 40–100 ms or 16 ms for $A17_{1–16}$ and $A17_{17–38}$ due to their lower solubility, with 40 μM A17, 10 μM D13, and 500 μM rifampicin. An NOESY spectrum with a 250-ms mixing time was acquired on a 1 mM sample of $A17_{1–38}$. For SPR experiments, His6-tagged D13 was immobilized on a Sensor Chip Biacore S-compatible NIHC 1500M (Xantec) and analyzed on a Biacore S200 (GE Healthcare).

ACKNOWLEDGMENTS. We are grateful for support of the respective beamline scientists. We thank M. Hijnen (GE Healthcare) for his technical help with SPR experiments and K. Erlandson and B. Moss (National Institute of Allergy and Infectious Diseases) for useful suggestions. We thank R. Wirasinha for her advice on the figures. Diffraction experiments were carried out on MX1 at Australian Synchrotron and X06DA at Swiss Light Source. Electron microscopy was performed at the Clive and Vera Ramaciotti Centre for Cryo Electron Microscopy. This project was supported by Project Grant APP1051907 of the Australian National Health and Medical Research Council. D.G. was the recipient of a Senior Postdoctoral Fellowship from Faculty of Medicine, Nursing and Health Sciences, Monash University; F.C. was the recipient of Future Fellowship FT120100893 from the Australian Research Council.

1. Colson P, et al. (2013) "Megavirales", a proposed new order for eukaryotic nucleocytoplasmic large DNA viruses. *Arch Virol* 158:2517–2521.
2. Moss B (2015) Poxvirus membrane biogenesis. *Virology* 479–480:619–626.
3. Suarez C, et al. (2015) African swine fever virus assembles a single membrane derived from rupture of the endoplasmic reticulum. *Cell Microbiol* 17:1683–1698.
4. Mutsafi Y, Shimoni E, Shimon A, Minsky A (2013) Membrane assembly during the infection cycle of the giant Mimivirus. *PLoS Pathog* 9:e1003367.
5. Condit RC, Moussatche N, Traktman P (2006) In a nutshell: Structure and assembly of the vaccinia virion. *Adv Virus Res* 66:31–124.
6. Hyun J-K, et al. (2011) Membrane remodeling by the double-barrel scaffolding protein of poxvirus. *PLoS Pathog* 7:e1002239.
7. Bahar MW, Graham SC, Stuart DI, Grimes JM (2011) Insights into the evolution of a complex virus from the crystal structure of vaccinia virus D13. *Structure* 19:1011–1020.
8. Maruri-Avidal L, Weisberg AS, Moss B (2013) Direct formation of vaccinia virus membranes from the endoplasmic reticulum in the absence of the newly characterized L2-interacting protein A30.5. *J Virol* 87:12313–12326.
9. Chlanda P, Carbajal MA, Cyrklaff M, Griffiths G, Krijnse-Locker J (2009) Membrane rupture generates single open membrane sheets during vaccinia virus assembly. *Cell Host Microbe* 6:81–90.
10. Chichón FJ, et al. (2009) Membrane remodelling during vaccinia virus morphogenesis. *Biol Cell* 101:401–414.
11. Erlandson KJ, et al. (2016) Poxviruses encode a reticulon-like protein that promotes membrane curvature. *Cell Rep* 14:2084–2091.
12. Bisht H, Weisberg AS, Szajner P, Moss B (2009) Assembly and disassembly of the capsid-like external scaffold of immature virions during vaccinia virus morphogenesis. *J Virol* 83:9140–9150.
13. Unger B, Mercer J, Boyle KA, Traktman P (2013) Biogenesis of the vaccinia virus membrane: Genetic and ultrastructural analysis of the contributions of the A14 and A17 proteins. *J Virol* 87:1083–1097.
14. Grimley PM, Rosenblum EN, Mims SJ, Moss B (1970) Interruption by rifampin of an early stage in vaccinia virus morphogenesis: Accumulation of membranes which are precursors of virus envelopes. *J Virol* 6:519–533.
15. Moss B, Rosenblum EN, Katz E, Grimley PM (1969) Rifampicin: A specific inhibitor of vaccinia virus assembly. *Nature* 224:1280–1284.
16. Hartmann G, Honikel KO, Knüsel F, Nüesch J (1967) The specific inhibition of the DNA-directed RNA synthesis by rifamycin. *Biochim Biophys Acta* 145:843–844.
17. Subak-Sharpe JH, Timbury MC, Williams JF (1969) Rifampicin inhibits the growth of some mammalian viruses. *Nature* 222:341–345.
18. Nagaya A, Pogo BG, Dales S (1970) Biogenesis of vaccinia: Separation of early stages from maturation by means of rifampicin. *Virology* 40:1039–1051.
19. Tartaglia J, Piccini A, Paoletti E (1986) Vaccinia virus rifampicin-resistance locus specifies a late 63,000 Da gene product. *Virology* 150:45–54.
20. Baldick CJ, Jr, Moss B (1987) Resistance of vaccinia virus to rifampicin conferred by a single nucleotide substitution near the predicted NH2 terminus of a gene encoding an Mr 62,000 polypeptide. *Virology* 156:138–145.
21. Charity JC, Katz E, Moss B (2007) Amino acid substitutions at multiple sites within the vaccinia virus D13 scaffold protein confer resistance to rifampicin. *Virology* 359:227–232.
22. Zhang Y, Moss B (1992) Immature viral envelope formation is interrupted at the same stage by lac operator-mediated repression of the vaccinia virus *D13L* gene and by the drug rifampicin. *Virology* 187:643–653.
23. Erlandson KJ, et al. (2014) Duplication of the A17L locus of vaccinia virus provides an alternate route to rifampin resistance. *J Virol* 88:11576–11585.
24. Tartaglia J, Paoletti E (1985) Physical mapping and DNA sequence analysis of the rifampicin resistance locus in vaccinia virus. *Virology* 147:394–404.
25. Sodeik B, Griffiths G, Ericsson M, Moss B, Doms RW (1994) Assembly of vaccinia virus: Effects of rifampin on the intracellular distribution of viral protein p65. *J Virol* 68:1103–1114.
26. Mayer M, Meyer B (1999) Characterization of ligand binding by saturation transfer difference NMR spectroscopy. *Angew Chem Int Ed Engl* 38:1784–1788.
27. Gossert AD, Jahnke W (2016) NMR in drug discovery: A practical guide to identification and validation of ligands interacting with biological macromolecules. *Prog Nucl Magn Reson Spectrosc* 97:82–125.
28. Grimley PM, Moss B (1971) Similar effect of rifampin and other rifamycin derivatives on vaccinia virus morphogenesis. *J Virol* 8:225–231.
29. Campbell EA, et al. (2001) Structural mechanism for rifampicin inhibition of bacterial RNA polymerase. *Cell* 104:901–912.
30. Wang D-R, et al. (2014) Vaccinia viral protein A27 is anchored to the viral membrane via a cooperative interaction with viral membrane protein A17. *J Biol Chem* 289:6639–6655.
31. Szajner P, Weisberg AS, Lebowitz J, Heuser J, Moss B (2005) External scaffold of spherical immature poxvirus particles is made of protein trimers, forming a honeycomb lattice. *J Cell Biol* 170:971–981.